Journal of Hazardous Materials 189 (2011) 556–563

Contents lists available at ScienceDirect

Journal of Hazardous Materials

journal homepage: www.elsevier.com/locate/jhazmat

Influence of natural organic matter on the aggregation and deposition of titanium dioxide nanoparticles

Beng Joo Reginald Thio, Dongxu Zhou, Arturo A. Keller*

Bren School of Environmental Science & Management, University of California, Santa Barbara, 3420 Bren Hall, Santa Barbara, CA 93106 – 5131, United States

ARTICLE INFO

Article history:
Received 28 November 2010
Received in revised form 21 February 2011
Accepted 22 February 2011
Available online 1 March 2011

Keywords:
TiO_2 nanoparticles
SRHA
QCM-D
Critical coagulation concentration
Aggregation kinetics
Deposition

ABSTRACT

The aggregation kinetics of TiO_2 nanoparticles was studied in the absence and presence of Suwanee River humic acid (SRHA) in either NaCl or $CaCl_2$ electrolytes. The CCC[Ca^{2+}]/CCC[Na^+] ratios were found to yield a proportionality fraction of $z^{-7.2}$ (in the absence of SRHA) and $z^{-5.6}$ (in the presence of SRHA), near the theoretical prediction of z^{-6}, where z is the cation's valence. SRHA drastically increased the stability of TiO_2 nanoparticles under most conditions, due to the combined effect of increased electrostatic and steric repulsions. Deposition rates of TiO_2 nanoparticles onto a silica surface were quantitatively measured using a quartz crystal microbalance with dissipation (QCM-D) over a broad range of solution (pH and ionic strength, *IS*) conditions, and the effects of the SRHA on particle deposition behavior were evaluated. In general, zeta potential can be used to predict the interaction energies between particles or particles and surfaces, and from there an inference can be made as to the potential for aggregation and deposition. The presence of SRHA significantly hinders TiO_2 deposition onto silica surfaces via steric repulsion in addition to repulsive electrostatics even under high ionic strength, which has important implications for the mobility of these nanoparticles.

1. Introduction

The key to understanding the environmental implications of different nanomaterials will be a robust predictive framework for their fate and transport, so that exposure (dose) can be estimated. The main questions that fate and transport studies must answer relate to nanoparticle mobility, persistence, bioavailability and reactivity. Nanoscale TiO_2 is widely used in commercial applications such as photocatalysts, ceramic membranes and cosmetic pigment additives [1]. The impact and possible risks of nanotechnology on the environment through the use of such engineered nanomaterials in society has lead to multiple studies on their fate and transport [2–5] as well as ecotoxicity in the event of exposure [6–8]. In particular, numerous studies have been done to quantify the environmental fate and behavior of TiO_2 nanoparticles [9–14]. While previous researchers have characterized the physicochemical properties and transport behavior of TiO_2 nanoparticles (NPs) over a range of environmentally relevant conditions under varying ionic strength (*IS*), pH and to some extent the interactions with natural organic matter (NOM), there is still a need to understand TiO_2 NP mobility and stability in complex aqueous matrices.

The mobility of NPs in the environment is controlled by their aggregation and deposition rates. Traditionally, the Derjaguin–Landau–Verwey–Overbeek (DLVO) theory [15] that has been considered is dependent on pH and ionic strength, since these two water chemistry parameters control the charge on the NP and the thickness of the electric double layer surrounding the particle. As the pH of the aqueous system approaches the point of zero charge (PZC), there is a marked decrease in the electrostatic repulsion between NPs or between a NP and the surrounding solid surfaces, resulting in a faster rate of aggregation, increased aggregate size, and increased rate of deposition onto soil and sediment particles. At any given pH, an increase in the ionic strength of the aqueous system results in a thinner electric double layer surrounding the NPs and the surrounding surfaces, again increasing the rate of aggregation, the size of the aggregates, and the rate of deposition onto mineral surfaces. While the NPs may aggregate to sub-micron or larger colloids [16], it is likely that many of the exposed surfaces still retain nanoscale properties (e.g., quantum effects, very high surface area) that can have environmental implications.

However, the presence of natural organic matter (NOM), composed of thousands of organic compounds (e.g. organic acids, sugars and other carbohydrates, cellulosic materials, alginate, proteins, lipids, etc.), in all natural aqueous matrices has a profound effect on the charge balance of the NPs, and thus on their mobility and deposition behavior [17–19].

* Corresponding author. Tel.: +1 805 453 1822; fax: +1 805 893 7612.
E-mail address: keller@bren.ucsb.edu (A.A. Keller).

0304-3894/$ – see front matter © 2011 Elsevier B.V. All rights reserved.
doi:10.1016/j.jhazmat.2011.02.072

The early-stage NP–NP aggregation kinetics (in practice treated as the time in which the aggregate's mean diameter grows by 50%) is believed to reflect the formation of doublets [20],

$$\left(\frac{da_h(t)}{dt}\right)_{t\to 0} \propto k_{11}N_0 \quad (1)$$

where $a_h(t)$ is the hydrodynamic diameter of aggregates as a function of time t, N_0 is the initial number concentration of primary particles, and k_{11} is the doublet formation rate. In the absence of NOM, under low salt concentration, k_{11} is sensitive to the change in ionic strength, since increase in ionic strength will diminish the energy barrier. At high salt concentration, the energy barrier is significantly diminished, and k_{11} will be equal to the diffusion-limited aggregation rate, k_{diff}. The NP–NP attachment efficiency, $\alpha = k_{11}/k_{diff}$, is used to describe the aggregation kinetics. The diffusion-limited (DLCA) and reaction-limited (RLCA) clustering aggregation regimes can be identified in a plot of electrolyte concentration vs. α, and the transition is denominated the critical coagulation concentration (CCC) [21]. The presence of NOM can significantly shift the CCC, since the effective charge on the particles is modified by the adsorbed NOM. Steric hindrance and other interactions may also affect the CCC. Electrostatic repulsion is controlled by two terms, surface potential and the Debye–Huckel parameter, $1/\kappa$. The Debye–Huckel parameter κ characterizes the exponential decay of the electrostatic repulsion. At 25 °C, κ can be calculated using [21],

$$\kappa = 2.32 \times 10^9 \left(\sum c_i z_i^2\right)^{1/2} \quad (2)$$

where c_i is the concentration of the ith ion, and z_i is the valence of the ith ion.

Similarly for deposition, there are conditions that lead to rapid deposition (e.g., positively charged particles attaching onto negatively charged surfaces), others that prevent deposition (e.g., particles and surfaces strongly negatively charged), and a transition regime as the charge on the particle is influenced by the cations in solution. NOM also plays a significant role in modifying the regime at which the system transitions from no deposition to rapid deposition.

The objective of this paper is to systematically examine the influence of NOM on the kinetics of TiO_2 NP aggregation and deposition onto silica surfaces, which are similar to those found in natural soils and sediments. Fatisson et al. [9] demonstrated the capability of the quartz crystal microbalance with dissipation monitoring (QCM-D) as an effective sensitive real-time tool to quantify the deposition of TiO_2 NP suspensions onto clean silica surfaces in aqueous media. However their study was performed at pH 3, 5 and 9 and without NOM; the results can be strikingly different under more realistic conditions with NOM present. For this study we dispersed TiO_2 NPs in several aqueous matrices and measured their deposition onto silica using QCM-D. These matrices represent a wide range of ambient water conditions, particularly with regard to *IS*, NOM and pH, and enable us to understand the factors that influence the mobility of TiO_2 NPs in the environment.

2. Experimental

2.1. Preparation of NP suspensions

TiO_2 NPs were acquired from Evonik Degussa Corp. (U.S.). The nominal diameter reported by the manufacturer was 30 nm. A detailed characterization of these NPs was presented previously [4]. A stock suspension of TiO_2 NPs (100 mg/L) was prepared by transferring the TiO_2 powder into deionized (DI) water followed by ultrasonication in a sonication bath (Branson 2510, Danbury, CT) for 30 min. TiO_2 suspensions (10 mg/L) were prepared by diluting the stock suspension into a number of NaCl and $CaCl_2$ (Sigma–Aldrich) solutions of different salt concentrations (*IS* = 1, 10 and 100 mM) at pH 5, 6, 7, 8 and 9. The resulting TiO_2 suspensions were further sonicated for another 15 min prior to use.

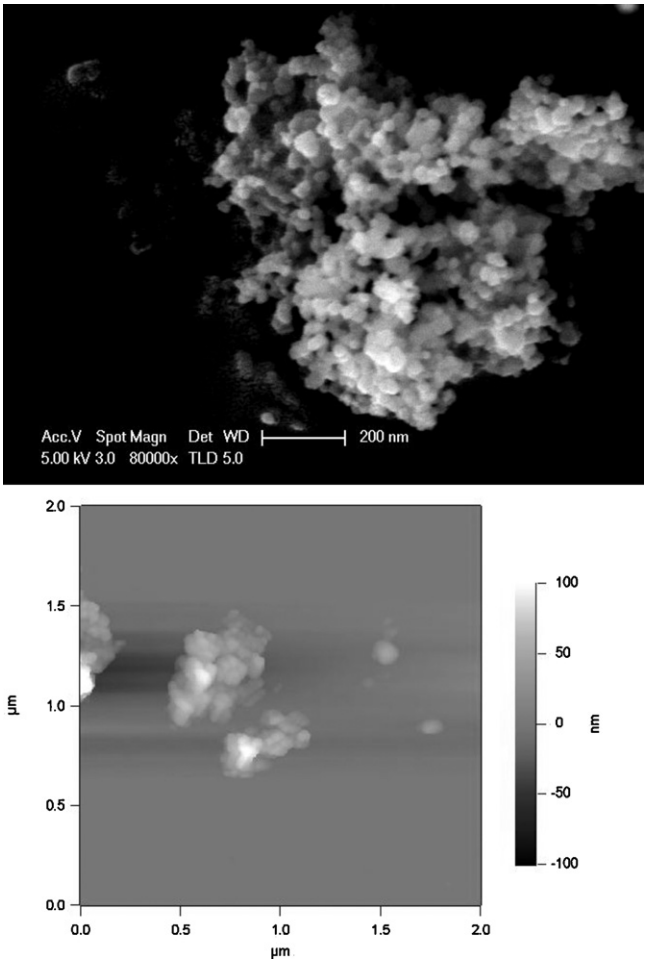

Fig. 1. Representative (a) SEM and (b) AFM images of dry, unused TiO_2 nanoparticles. Both images show particles to be roughly spherical and around 40–60 nm in primary diameter.

We used Suwanee River humic acid (SRHA, Standard II, International Humic Substances Society) as model for naturally occurring humic substances. Humic acid stock solution (100 mg/L) was prepared by dissolving the humic acid in DI water and then further diluting to 10 mg/L with the TiO_2 suspensions.

2.2. NP sizing and imaging

Scanning electron microscopy (SEM) (XL40 Sirion FEG Digital Scanning Microscope w/EDS, FEI company, Hillsboro, OR) and atomic force microscopy (AFM) (MFP-3D, Asylum Research, Santa Barbara, CA) were used to characterize the primary size of the dry TiO_2 NPs as received from the manufacturer. Examination by both SEM and AFM revealed that the TiO_2 NPs are roughly spherical and about 40–60 nm in diameter (Fig. 1). Dynamic light scattering (DLS, Malvern Zetasizer Nano ZS-90) was used to measure the hydrodynamic diameter of the TiO_2 particles under various solution chemistries. The particles were sonicated prior to the DLS measurement.

2.3. Zeta potential

Laser Doppler velocimetry (Malvern Zetasizer Nano ZS-90) was used to characterize the electrophoretic mobility (EPM) of the TiO_2 NPs in the various electrolytes. Measured EPMs were converted to ζ-potential using the Smoluchowski equation. 200 nm SiO_2 particles (Brinker Nanostructures Research Group, University of New Mexico) were used as a surrogate to characterize the ζ-potential of the silica surface of the QCM-D sensor crystal. This method is similar to the one used by Jiang et al. [22] in their measurements of the ζ-potentials of crushed SRHA-coated and uncoated quartz sand as substitutes for the ζ-potentials of silica surfaces and surfaces precoated with SRHA of their QCM-D.

2.4. Aggregation kinetics

The hydrodynamic size of TiO_2 NPs was determined as a function of time using dynamic light scattering (DLS) (Zetasizer nano, Malvern Instruments) with a 633 nm laser source and a detection angle of 90°. An aliquot of stock suspension was withdrawn and sonicated for 10 min to re-disperse the particles. Borate buffer with preadjusted pH of 8 and humic acid stock solution were added to achieve a final buffer concentration of 1 mM and final humic acid concentration of 10 mg/L. A measured amount of Nanopure water was then used to dilute the sample. Immediately after adding the desired amount of electrolytes, DLS measurements were started. Data was collected at 30 s intervals, and the intensity weighted mean hydrodynamic radius was collected for sample analysis. Data collection was continued until a 50% increase in the hydrodynamic radius was observed.

2.5. Quartz crystal microbalance with dissipation

A QCM-D D300 system (Q-Sense AB, Gothenburg, Sweden) was used to examine the deposition behavior of TiO_2 NPs on silica surfaces. QCM-D experiments were performed by simultaneously monitoring the changes in frequency (Δf) and energy dissipation (ΔD) of a 5 MHz AT-cut quartz sensor crystal with silica coated surface (QSX-303). Before use, the crystal, chamber and tubing were cleaned by rinsing with at least 10 mL DI water and 5 mL of ethanol. The crystal was further cleaned in a UV–ozone chamber for 30 min before being mounted onto the chamber. The TiO_2 NP deposition experiments were performed in batch mode at a preset temperature of 298 K. A background electrolyte (1 mL) at the pH and ionic strength of interest was injected into the QCM-D chamber for a minimum of 1 h or until a stable baseline was obtained (drift of average normalized frequency less than 0.2 Hz within 30 min), whichever was longer. Subsequently, 0.5 mL of the TiO_2 suspension in the same electrolyte was injected into the chamber and the Δf and ΔD were recorded. In our study, we monitored the shifts in the normalized third overtone frequency and dissipation (Δf_3 and ΔD_3) since this overtone usually has the best signal-to-noise ratio [23] to determine the TiO_2 deposition behavior onto silica in different electrolyte types and concentrations (*IS*). The working volume of the D300 chamber is 80 μL [24], and 0.5 mL of TiO_2 suspension is sufficient to displace the background electrolyte completely. QCM-D experiments were repeated using at least three different samples (prepared on different days) of each unique electrolyte concentration and pH.

In cases where deposition of TiO_2 onto the silica surface occurs as very thin or quasi-rigid layers, the increase in the mass per unit area Δm can be described by the Sauerbrey relationship [25]:

$$\Delta m = -\frac{C\Delta f_n}{n} \quad (3)$$

Table 1
Comparison of the mass of TiO_2 deposited on QCM-D silica surface (1 cm^2) determined by ICP and Sauerbrey relationship.

Δf_3	Mass of TiO_2 by ICP (μg)	Mass of TiO_2 by Sauerbrey relationship (μg)
0	0.00	0.000
−1.5	1.63	0.0089
−3	1.95	0.018
−7	2.28	0.041
−8	2.32	0.047

where Δf_n is the shift in resonance overtone frequency, n is the overtone number (1, 3, 5, or 7) and C is the mass sensitivity constant (17.7 ng/cm^2/Hz when f = 5 MHz). ΔD_n is calculated using the Q-sense software (Qsoft) and can be described as the ratio of the energy lost during one oscillation cycle to the total energy stored in the oscillator at a resonance overtone frequency n. ΔD provides complementary information with the Δf on the deposition process as well as some of the viscoelastic properties of the deposited layer. In general, a negative Δf and a positive ΔD mean particle deposition onto the silica surface occurs, while the reverse is true in cases of particles detaching from the silica surface. In our study, we monitored the shifts in the normalized third overtone frequency and dissipation (Δf_3 and ΔD_3) since this overtone usually has the best signal-to-noise ratio [23] to determine the TiO_2 deposition behavior onto silica in different electrolyte types and concentrations (*IS*).

2.6. Inductively coupled plasma atomic emission spectroscopy (ICP-AES)

A Thermo iCAP 6300 ICP was used to measure the concentration of several of the TiO_2 suspensions before and after passing through the QCM-D chamber. The difference in concentration was used to determine the mass of TiO_2 deposited on the silica surface, and was compared to calculations of mass deposited using the Sauerbrey relation from the raw QCM-D data (Table 1). Briefly, 0.5 mL of the TiO_2 suspension was collected on a test-tube and the volume diluted with DI water to 5 mL. A 0.1136 mL H_2SO_4–$(NH_4)_2SO_4$ mixture (2.976 g of $(NH_4)_2SO_4$, 4 mL DI water, 6 mL conc. H_2SO_4) was added to the test tube, put on high heat on a heating plate for 1 h and cooled for 5 min. 0.1420 mL conc. HNO_3 and 0.4261 mL conc. HCL were then added to the resulting mixture and let sit for another 10 min before being injected into the ICP. Elemental standard solution (1000 mg/L Ti, Merck, Darmstadt, Germany) was employed to prepare diluted standard solutions to ICP-AES optimization.

3. Results and discussion

3.1. Electrophoretic mobility measurements

Fig. 2 presents the ζ-potentials of TiO_2 NPs in the absence of SRHA. For reference, the ζ-potential as a function of pH under very low *IS*, used to determine the pH at PZC (pH_{pzc}) is shown in Fig. 3. ζ-potentials of the TiO_2 particles in the presence of monovalent NaCl ranged from +20 mV at pH 4 to −50 mV at pH 9 at 1 mM *IS*, which are similar to previously reported studies [9,14], and became less positive or more negative with the increase of *IS* due to the compression of the electrostatic double layer. However, the trend of ζ-potential for $CaCl_2$ at the same *IS* and pH does not follow the screening of the double layer, indicating that Ca^{2+} is a potential determining ion (particularly at 10 and 100 mM [Ca^{2+}]) rather than an indifferent ion. ζ-potentials were either less positive (at pH < pH_{pzc}) or less negative (pH > pH_{pzc}) at higher *IS* (Fig. 2b) suggesting that as more Ca^{2+} ions surround the TiO_2 NPs, they neutralize the surface charge (pH 8, Fig. 4), or shorten the Debye length with increased ion valence and *IS* (Fig. 5) and thus result in smaller TiO_2 electrostatic repul-

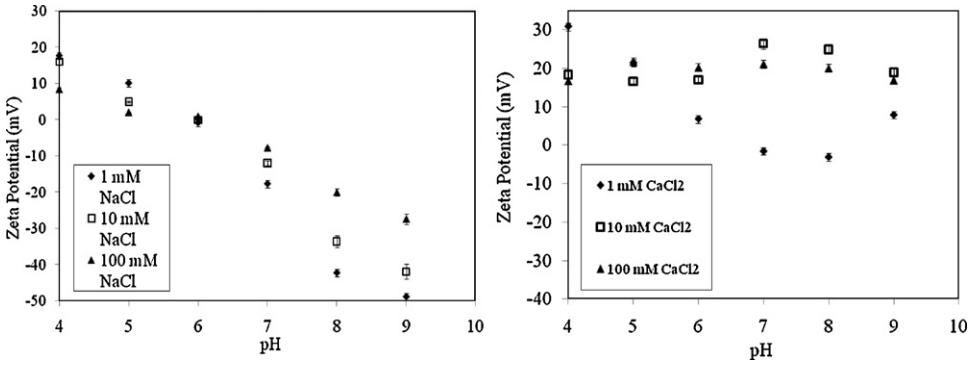

Fig. 2. ζ-potential of TiO_2 nanoparticles at different pHs and *IS*: (a) in NaCl; (b) in $CaCl_2$.

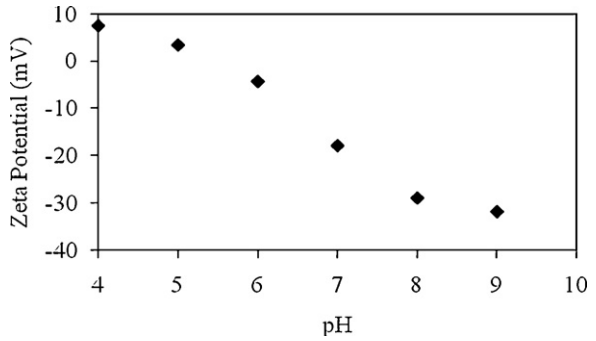

Fig. 3. ζ-Potential of TiO_2 nanoparticles as a function of pH in the absence of electrolytes and SRHA.

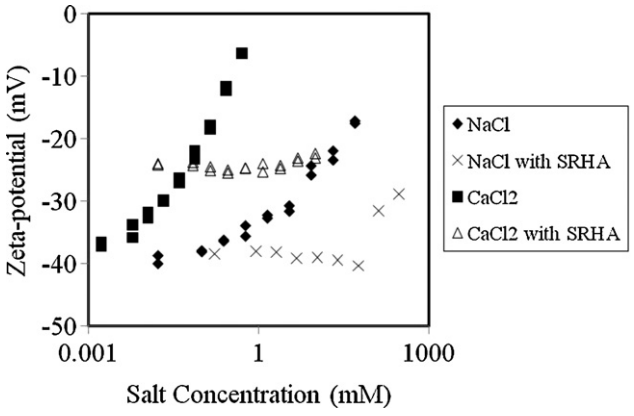

Fig. 4. Salt titration of TiO_2 vs. zeta-potential at pH 8, for NaCl and $CaCl_2$, with and without Suwanee River humic acid (SRHA).

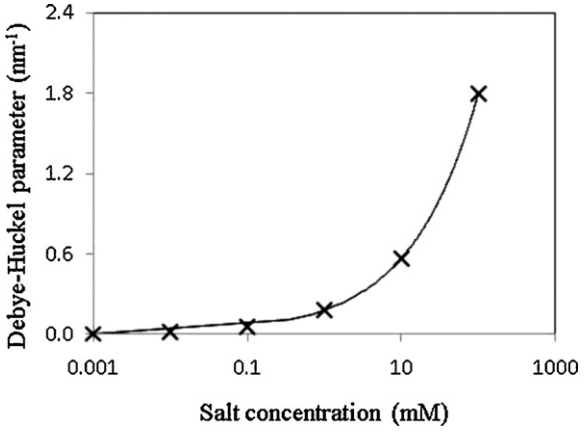

Fig. 5. Debye–Huckel parameter as a function of $CaCl_2$ concentration.

sion potentials [14]. The presence of Ca^{2+} has generally increased the net positive charge on the TiO_2 nanoparticle suspension [10].

In the presence of SRHA, the ζ-potentials of TiO_2 NPs are negative at $4 < pH < 9$ regardless of *IS* and type of electrolyte (Fig. 6). This indicates the properties of the TiO_2 NPs are significantly modified by the adsorption of SRHA to the particle surfaces. Although higher *IS* leads to a decrease in the magnitude of the ζ-potentials due to the compression of the double layer around the TiO_2 NPs, the effect is much weaker. The decrease in magnitude of ζ-potentials is more pronounced in the case of $CaCl_2$ than NaCl, reflecting the effect of ion valence on particle surface charge.

For reference, the ζ-potentials of silica particles for $5 < pH < 9$ in the presence of $CaCl_2$ and SRHA are presented in Fig. 7 and are negatively charged. At higher *IS*, the ζ-potentials of silica become less negative, indicating the increased screening of the surface charges. Our results show the stronger effect of Ca^{2+} over the SRHA and pH. The ζ-potentials suggest that the Ca^{2+} ions can act as electrostatic bridges between the negatively charged silica nanoparticles at a pH range of 7–9. In addition, there is the effect of ion valence on the Debye length and in turn, on electrostatic repulsion. From Eq. (2) the inverse of the Debye length is proportional to the valence charge of the ion; as valence charge increases ($z = 2$ for Ca^{2+} and $z = 1$ for Na^+) the Debye length decreases resulting in smaller magnitude Zeta-potentials. This phenomenon is in agreement with the previous report by French et al. [14].

3.2. Aggregation kinetics of TiO_2 NPs

TiO_2 nanoparticles were observed to form stable suspensions with aggregates of radius 100–200 nm after dispersion in Nanopure water. The stock suspension prepared in this study was stable for more than 4 days without change in aggregate size as mea-

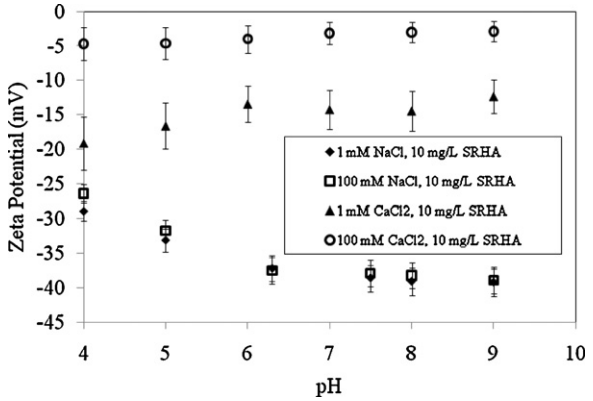

Fig. 6. ζ-Potential of TiO_2 with Suwanee River humic acid (SRHA) as a function of pH, in various electrolytes and ionic strengths.

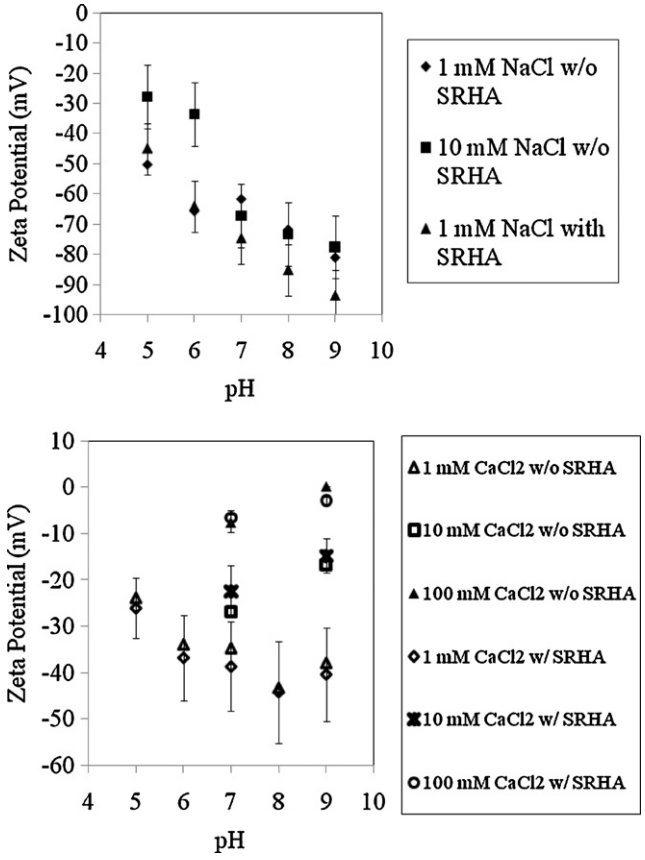

Fig. 7. ζ-Potential of silica nanoparticles as a function of pH in varying concentrations of (a) NaCl and (b) $CaCl_2$ and presence/absence of SRHA.

sured by DLS. Similar behavior was observed in previous studies [14,16,26,27], and it is proposed that the enhanced collision frequency due to the local high particle concentration when the stock dispersion was prepared and the reduced surface energy when forming larger aggregates could be the driving forces of this phenomenon. Fig. 8 shows a representative aggregation profile at pH 8 with five different $CaCl_2$ concentrations. At low $CaCl_2$ concentration (0.01, 0.05, and 0.1 mM), an increase in ionic strength led to faster aggregation, which is ascribed to the screening of the electric double layer. At higher $CaCl_2$ concentration (1, 10 mM)), further increase in ionic strength had no effect in enhancing aggregation.

The DLCA and RLCA regimes were identified for the four conditions tested (Fig. 9). In the absence of humic acid, the CCC was ca. 15 mM for NaCl electrolyte, while it was only ca. 0.1 mM for

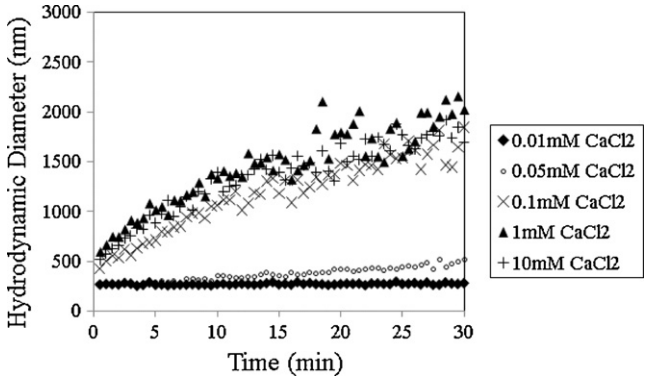

Fig. 8. Representative time-resolved aggregation data of TiO_2 nanoparticles. [TiO_2] = 100 mg/L, pH 8.

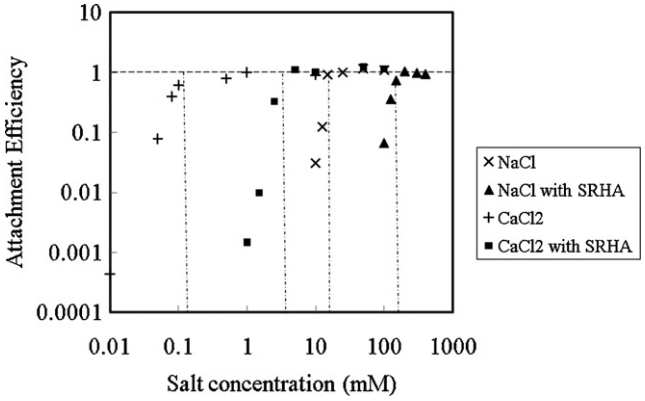

Fig. 9. Attachment efficiency of TiO_2 at four conditions. [TiO_2] = 100 mg/L, pH 8 [SRHA] = 10 mg/L (when present).

$CaCl_2$. In the presence of humic acid, the CCC was ca. 200 mM for NaCl electrolyte, compared with ca. 5 mM for $CaCl_2$ electrolyte. The CCC[Ca^{2+}]/CCC[Na^+] ratio yields a proportionality fraction of $z^{-7.2}$ (in the absence of humic acid) and $z^{-5.3}$ (in the presence of humic acid), where z is the cation's valence. The Shultz–Hardy trend predicts a proportionality fraction of z^{-6} for systems without cation specific adsorption [27], however, due to the limited data size, no conclusion can be drawn regarding the statistical significance of the difference between the experimental and the theoretical values. The addition of humic acid clearly stabilized TiO_2 particles, evidenced by the increase of CCC over an order of magnitude. Zeta-potential measurements revealed that in the absence of humic acid, the surface charge of TiO_2 is sensitive to *IS*, the addition of either NaCl or $CaCl_2$ leads to smaller zeta-potential values, and Ca^{2+} is more effective in depressing the surface charge of TiO_2 (Fig. 4).

The role of the cations in destabilizing TiO_2 particles in the absence of humic acid is two-fold: (1) reduce the surface charge of TiO_2 NPs; and (2) lessen the exponential decay length (i.e., Debye length) of the electrostatic repulsion. In contrast, in the presence of humic acid, increasing *IS* has much less effect on surface charge of TiO_2 NPs, since the TiO_2 surface is covered by humic acid and the measured zeta-potential represents the properties of the humic acid (Fig. 4). In this case salt induces aggregation solely by compressing the electric double layer. In addition, humic acid coated TiO_2 is more resistant to salt induced aggregation due to salt enhanced humic acid adsorption on TiO_2. It is suggested that humic substances would become more coiled and compact with increased ionic strength [19,28]. Consequently greater amount of humic substance could adsorb onto the surface of nanoparticles and lead to enhanced steric hindrance.

Chen et al. [20] reported enhanced aggregation of alginate-coated hematite in the presence of calcium ions, possibly due to the formation of an alginate gel network enhanced by calcium complexation, which bridged the hematite clusters. In their study, $CaCl_2$ concentration was shown to be positively related to the apparent attachment efficiency. Similar behavior was not observed for the SRHA–Ca^{2+}–TiO_2 system in this study, indicating the different response towards Ca^{2+} between SRHA and alginate. Using Chen et al.'s method [20], the aggregation rate constant under diffusion-limited conditions (k_{11}) were calculated for the four conditions tested (6.3×10^{-19} m^3/s (NaCl), 7.5×10^{-19} m^3/s (NaCl with SRHA), 1.23×10^{-18} m^3/s ($CaCl_2$), 6.56×10^{-19} m^3/s ($CaCl_2$ with SRHA)). These comparable k_{11} values suggest that regardless of the cation that is present, under diffusion-limited conditions the TiO_2 nanoparticles aggregate at the same rate within the experimental error.

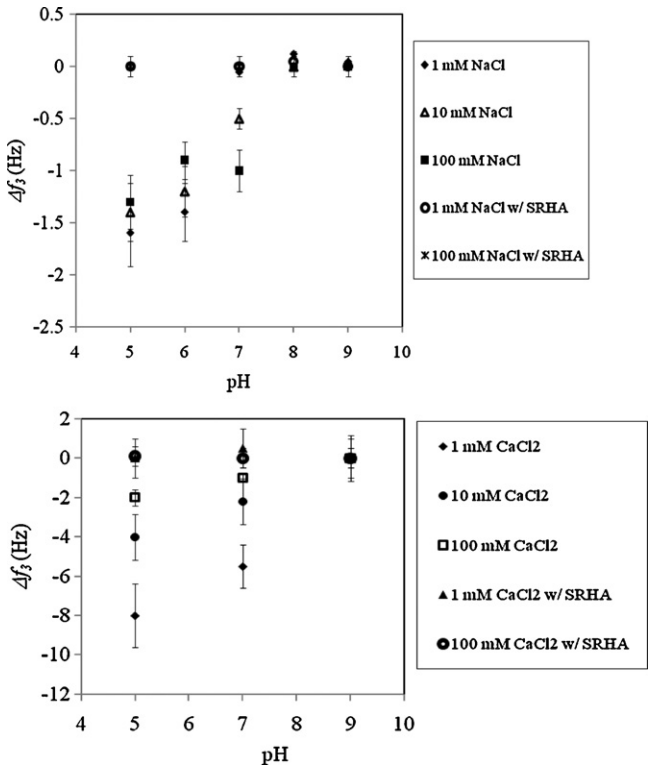

Fig. 10. Frequency shift Δf_3 as a function of pH, IS and [SRHA]: (a) in NaCl; (b) in $CaCl_2$.

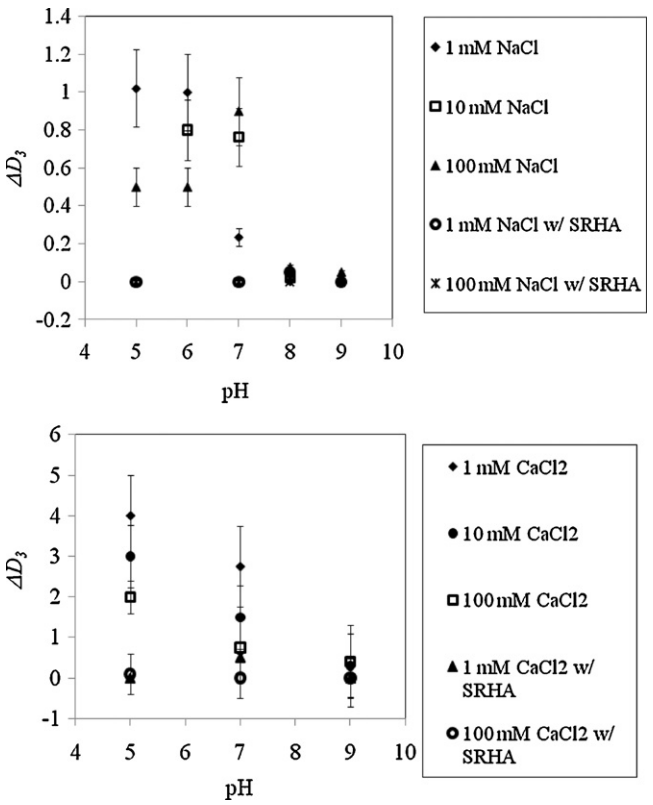

Fig. 11. Dissipation ΔD_3 as a function of pH, IS and [SRHA]: (a) in NaCl; (b) in $CaCl_2$.

3.3. TiO_2 deposition onto silica

Figs. 10 and 11 show the summary Δf_3 and ΔD_3 for the series of QCM experiments involving the deposition of TiO_2 NPs onto silica in NaCl and $CaCl_2$ at various *IS* and pH, while Fig. 12 shows a representative Δf_3 and ΔD_3 of TiO_2 deposition onto silica. In the case of NaCl, the magnitude of deposition, as measured by the Δf_3 and ΔD_3, decreases as pH increases; when pH is held constant ($5 < pH < 7$), an increase in *IS* from 1 to 100 mM has the same effect of decreasing deposition. At pH 8 and 9, we did not observe any TiO_2 deposition onto the silica surface regardless of *IS*. These behaviors are in qualitative agreement with the classical DLVO theory of colloidal stability [21,29,30]. For those experimental conditions where there was no deposition, we collected the data for a longer time period of 30 min beyond the introduction of the NPs into the chamber as shown in Fig. 13 to verify that the NP concentrations we were using were low enough such that gravity did not play a significant role in the deposition behavior. From Fig. 2, the ζ-potential of TiO_2 without SRHA in NaCl is nearly zero at pH 6 independent of *IS*, and becomes more positive as $pH \rightarrow 4$ and more negative as $pH \rightarrow 9$. Positive ζ-potentials of TiO_2 at $pH < 6$ mean that the attractive electrostatic forces predominate under such conditions; from Fig. 7 the silica surface is negatively charged under the range of conditions studied since its pH_{zpc} 3 [31]. At a fixed *IS*, the particles are more positively charged as the pH is decreased from pH 6 to pH 5 leading to increased deposition (Δf_3 becomes more negative and ΔD_3 more positive). As the *IS* increases from 1 to 100 mM NaCl, the electrostatic attraction between particles and surface is weakened and leads to smaller Δf_3 and ΔD_3 values. Our results are similar to that of Fatisson et al. [9], who used $NaNO_3$ as their monovalent electrolyte; however, they only studied the deposition at pH 3, 5 and 9, somewhat outside the range of environmentally relevant pH conditions. Conversely at $pH > 6$, repulsive electrostatic interactions dominate the NP-surface interactions and reduce or prevent TiO_2 deposition onto silica at all *IS*. At pH 7, the TiO_2 NPs in NaCl are negatively charged. As the *IS* increases from 1 to 100 mM NaCl, there is an increase in deposition shown by larger Δf_3 and ΔD_3 as repulsive forces are reduced due to the compression of the double layer by increased electrolyte concentration. Δf_3 and ΔD_3 were essentially zero at pH 8 and pH 9 at all *IS*, indicating no TiO_2 deposition.

When the electrolyte was switched to divalent $CaCl_2$, we observed a similar trend in TiO_2 deposition. The magnitude in deposition as indicated by Δf_3 and ΔD_3 of the TiO_2 in $CaCl_2$ was markedly higher than in NaCl at the same *IS*, reflecting the stronger electrostatic attraction of positively charged NPs and a negative

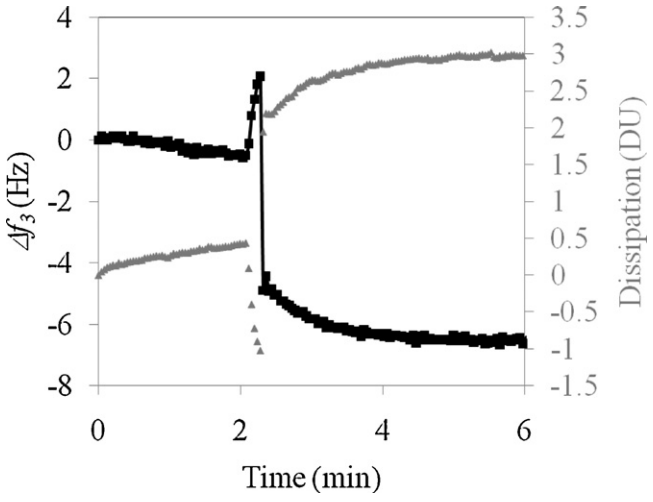

Fig. 12. Representative frequency shift (Δf_3) and dissipation (D_3) when TiO_2 nanoparticles are introduced to the QCM-D chamber with a silica coated sensor crystal in 1 mM $CaCl_2$ at pH 7.

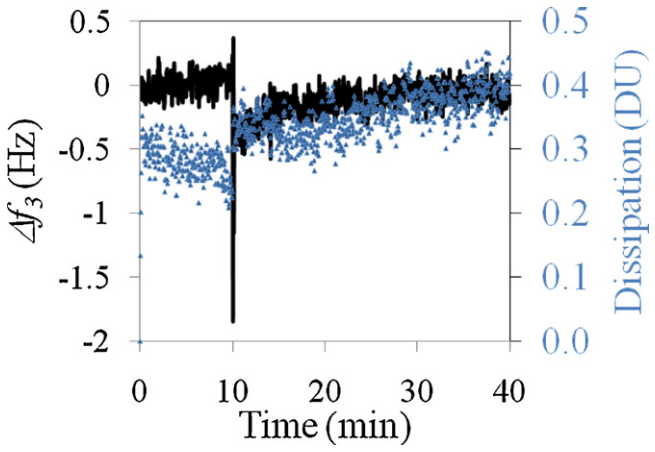

Fig. 13. Representative frequency shift (Δf_3) and dissipation (ΔD_3) when TiO_2 nanoparticles are introduced to the QCM-D chamber with a silica coated sensor crystal in 100 mM $CaCl_2$ at pH 7 with 10 mg/L SRHA.

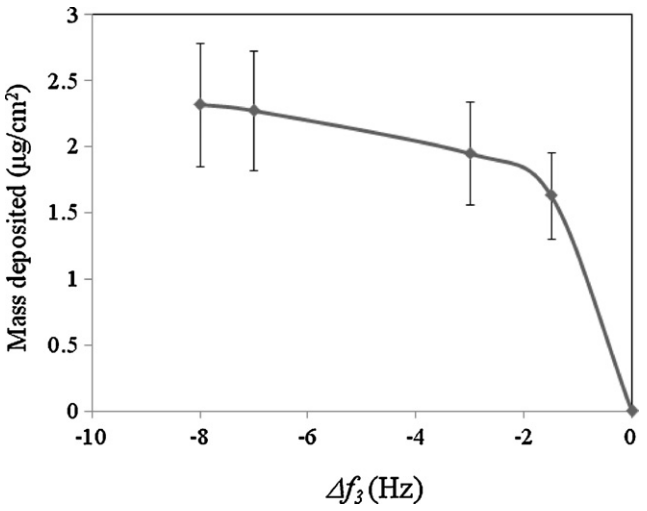

Fig. 15. Mass of TiO_2 deposited on silica surface determined using ICP as a function of Δf_3.

silica surface at pH 5 and 7 (Figs. 2b and 7). Higher [Ca^{2+}] leads to neutralization of the negative charges on the silica surface and thus to a reduction of electrostatic repulsive forces.

From Fig. 10b, the highest deposition (i.e. deposition efficiency) occurs at pH 5 and 1 mM $CaCl_2$ with a $|\Delta f_3|_{max}$ value of about 8 Hz. By normalizing the deposition behavior of the TiO_2 nanoparticles at other conditions with the $|\Delta f_3|_{max}$ value, we obtained a series of values for the TiO_2 deposition efficiency onto silica (Fig. 14). We show that the transition to no deposition for the TiO_2 nanoparticles onto silica occurred between 1 and 10 mM $CaCl_2$ at pH 5 and 7. In the case where NaCl was the electrolyte, the TiO_2 deposition efficiencies were all very low, with the transition regime occurring at below 1 mM NaCl which is not environmentally relevant (graph not shown). Given that most natural waters are in the pH range from 6 to 9, one would thus expect that in the presence of significant [Ca^{2+}], TiO_2 nanoparticles would not attach strongly to silica surfaces if NOM is not taken into consideration.

3.4. Effect of Suwanee River humic acid on TiO_2 deposition

In the presence of 10 mg/L SRHA at electrolyte concentrations of 1 mM and 100 mM NaCl and $CaCl_2$ from pH 5 to 9 (Figs. 10 and 11), no significant frequency or dissipation shifts were observed when the TiO_2 NPs were introduced. This indicates that the NP aggregates do not attach onto the silica surfaces when SRHA is present, which agrees well with previous reported results of the non-deposition

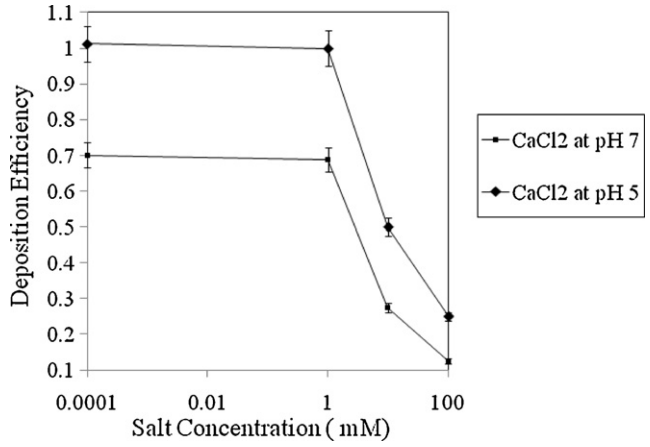

Fig. 14. Deposition efficiency of TiO_2 nanoparticles under various *IS* and pH conditions.

of engineered polymer modified NPs in the presence of organic macromolecules [32,33]. Given the negative zeta potential of the TiO_2 NPs in the presence of SRHA, it is not surprising that no deposition occurs, even at lower pH. Steric hindrance may also play a role, but it would be difficult to separate its contribution. Our results are similar to that previously reported by Chen and Elimelech [17] on the significant decrease in deposition of fullerene NPs on silica precoated with humic acid compared to the case where humic acid was absent. In their work, the adsorption of humic acid onto both fullerene NPs and silica surfaces prevented deposition, possibly due to steric repulsion thus, although possible also due in part to electrostatic repulsion of the two surfaces coated with humic acid.

3.5. Determination of TiO_2 mass deposition using ICP

Fig. 15 shows the relationship between the mass deposited on the silica surface determined using ICP with Δf_3. While the TiO_2 mass deposited on silica is non-linear with respect to Δf_3, the relationship can still be used to quantitatively determine the deposition rate under different environmental conditions. To our knowledge this is the first quantitative use of QCM-D for measuring deposition rates. The ICP measurements show that Δf_3 shifts of as low as 1.5 Hz correspond to deposition of TiO_2 NPs in the μg range, which are two orders of magnitude larger than that determined using the commonly used theoretical Sauerbrey [25] relationship (Table 1). This indicates the invalidity of using the Sauerbrey equation for non-homogeneous films since it underestimates the actual deposited mass for our system.

4. Conclusions

The aggregation kinetics and deposition behavior of nano-TiO_2 onto silica is a rather complex process that depends on the nature of the surfaces and the environmentally relevant solution pH [NOM] and IS. In our study, the TiO_2 nanoparticles were found to aggregate immediately upon their introduction to water, with the smallest aggregates slightly above 250 nm in hydrodynamic diameter. However, the presence of humic acid significantly stabilized the TiO_2 NPs. In the natural water matrices reported in a previous study [4], Na^+ is the dominant cation with a concentration above 400 mM in seawater samples, while Ca^{2+} is the predominate cation in groundwater and river water samples with a concentration in the range of 4–10 mM. All the natural waters had substantial concentration

of NOM. If NOM is not taken into consideration, one would predict that, given the IS in these natural waters, TiO_2 NPs would be in the diffusion-limited clustering aggregation regime, i.e., TiO_2 would undergo fast aggregation. However, since humic substances are present in all these waters, the combined effect of electrostatic repulsion and steric repulsion should stabilize the TiO_2 particles in these media, increasing their mobility. *IS* does play a role, but only for highly saline environments. Similarly, deposition of TiO_2 onto silica can be expected at lower pH in the absence of humic acids. However, in the presence of humic acid attachment of the TiO_2 onto silica surfaces is not favorable, regardless of pH and *IS*, and may not occur in the absence of other mechanisms, such as physical straining. Thus, NOM plays a very important role in determining the mobility of TiO_2 NPs in natural aqueous matrices.

Acknowledgements

This work was supported in part by the National Science Foundation and the US Environmental Protection Agency under Cooperative Agreement NSF-EF0830117. Any opinions, findings, and conclusions or recommendations expressed in this material are those of the authors and do not necessarily reflect the views of the National Science Foundation or the US Environmental Protection Agency. The research was also partly supported by the UC Toxic Substances Research and Training Program, Lead Campus on Nanotoxicology. We are grateful to Jacob Israelachvili for providing us with access to the QCM-D instrument (D300, Q-Sense AB), and to John Conway, Gabriel Rubio and Arjan Gower for assisting in collecting the ζ-potential data of the TiO_2 suspensions in various electrolyte concentrations. We also thank Casey Leavitt for collecting data on TiO_2 CCC and Ingmar Prokop for the QCM-D measurements.

References

[1] M.R. Wiesner, G.V. Lowry, P. Alvarez, D. Dionysiou, P. Biswas, Assessing the risks of manufactured nanomaterials, Environ. Sci. Technol. 40 (2006) 4336–4345.
[2] M.R. Wiesner, G.V. Lowry, K.L. Jones, M.F. Hochella Jr., R.T. Di Giulo, E. Casman, E.S. Bernhardt, Decreasing uncertainties in assessing environmental exposure, risk, and ecological implications of nanomaterials, Environ. Sci. Technol. 43 (2009) 6458–6462.
[3] H.A. Godwin, K. Chopra, K.A. Bradley, Y. Cohen, B.H. Harthorn, E.M.V. Hoek, P. Holden, A.A. Keller, H.S. Lenihan, R.M. Nisbet, A.E. Nel, The university of California center for the environmental implications of nanotechnology, Environ. Sci. Technol. 43 (2009) 6453–6457.
[4] A.A. Keller, H. Wang, D. Zhou, H.S. Lenihan, G. Cherr, B.J. Cardinale, R. Miller, Z. Ji, Stability and aggregation of metal oxide nanoparticles in natural aqueous matrices, Environ. Sci. Technol. 44 (2010) 1962–1967.
[5] X. Liu, M. Wazne, C. Christodoulatos, K.L. Jasinkiewicz, Aggregation and deposition behavior of boron nanoparticles in porous media, J. Colloid Interface Sci. 330 (2009) 90–96.
[6] B. Wu, Y. Wang, Y.-H. Lee, A. Horst, Z. Wang, D.-R. Chen, R. Sureshkumar, Y.J. Tang, Comparative eco-toxicities of nano-ZnO particles under aquatic and aerosol exposure modes, Environ. Sci. Technol. 44 (2010) 1484–1489.
[7] X. Liu, D. Vinson, D. Abt, R.H. Hurt, D.M. Rand, Differential toxicity of carbon nanomaterials in *Drosophila*: larval dietary uptake is benign, but adult exposure causes locomotor impairment and mortality, Environ. Sci. Technol. 43 (2009) 6357–6363.
[8] K. Tiede, M. Hassellov, E. Breitbarth, Q. Chaudhry, A.B.A. Boxall, Considerations for environmental fate and ecotoxicity testing to support environmental risk assessments for engineered nanoparticles, J. Chromatogr. A 1216 (2009) 503–509.
[9] J. Fatisson, R.F. Domingos, K.J. Wilkinson, N. Tufenkji, Deposition of TiO_2 nanoparticles onto silica measured using a quartz crystal microbalance with dissipation monitoring, Langmuir 25 (2009) 6062–6069.
[10] R.F. Domingos, C. Peyrot, K.J. Wilkinson, Aggregation of titanium dioxide nanoparticles: role of calcium and phosphate, Environmental Chemistry 7 (2009) 61–66.
[11] R.F. Domingos, N. Tufenkji, K.J. Wilkinson, Aggregation of titanium dioxide nanoparticles: role of fulvic acid, Environ. Sci. Technol. 43 (2009) 1282–1286.
[12] J. Kim, W. Shan, S.H.R. Davies, M.J. Baumann, S.J. Masten, V.V. Tarabara, Interactions of aqueous NOM with nanoscale TiO_2: implications for ceramic membrane filtration–ozonation hybrid process, Environ. Sci. Technol. 43 (2009) 5488–5494.
[13] K.A.D. Guzman, M.P. Finnegan, J.F. Banfield, Influence of surface potential on aggregation and transport of titania nanoparticles, Environ. Sci. Technol. 40 (2006) 7688–7693.
[14] R.A. French, A. Jacobson, B. Kim, S.L. Isley, R.L. Penn, P.C. Baveye, Influence of ionic strength, pH, and cation valence on aggregation kinetics of titanium dioxide nanoparticles, Environ. Sci. Technol. 43 (2009) 1354–1359.
[15] B.J.R. Thio, J.H. Lee, J.C. Meredith, A.A. Keller, Measuring the influence of solution chemistry on the adhesion of Au nanoparticles to mica using colloid probe atomic force microscopy, Langmuir 26 (2010) 13995–14003.
[16] D. Zhou, A.A. Keller, Role of morphology in the aggregation kinetics of ZnO nanoparticles, Water Res. 44 (2010) 2948–2956.
[17] K.L. Chen, M. Elimelech, Interaction of fullerene (C60) nanoparticles with humic acid and alginate coated silica surfaces: measurements, mechanisms, and environmental implications, Environ. Sci. Technol. 42 (2008) 7607–7614.
[18] K.L. Chen, M. Elimelech, Influence of humic acid on the aggregation kinetics of fullerene (C_{60}) nanoparticles in monovalent and divalent electrolyte solutions, J. Colloid Interface Sci. 309 (2007) 126–134.
[19] T. Phenrat, J. Song, C. Cisneros, D. Schoenfelder, R. Tilton, G.V. Lowry, Estimating attachment of nano- and submicrometer-particles coated with organic macromolecules in porous media: development of an empirical model, Environ. Sci. Technol. 44 (2010) 4531–4538.
[20] K.L. Chen, S.E. Mylon, M. Elimelech, Aggregation kinetics of alginate-coated hematite nanoparticles in monovalent and divalent electrolytes, Environ. Sci. Technol. 40 (2006) 1516–1523.
[21] M. Elimelech, R. Williams, J. Gregory, X. Jia, Particle Deposition and Aggregation, Butterworth–Heinemann, Oxford, UK, 1998.
[22] X. Jiang, M. Tong, H. Li, K. Yang, Deposition kinetics of zinc oxide nanoparticles on natural organic matter coated silica surfaces, J. Colloid Interface Sci. 350 (2010) 427–434.
[23] D. Xu, C. Hodges, Y. Ding, S. Biggs, A. Brooker, D. York, A QCM study on the adsorption of colloidal laponite at the solid/liquid interface, Langmuir 26 (2010) 8366–8372.
[24] Anonymous, Q-Sense Specifications D300 (2009).
[25] G. Sauerbrey, Verwendung Von Schwingquarzen Zur Wagung Dunner Schichten Und Zur Mikrowagung, Z. Phys. 155 (1959) 206–222.
[26] T. Phenrat, N. Saleh, K. Sirk, R. Tilton, G.V. Lowry, Aggregation and sedimentation of aqueous nanoscale zerovalent iron dispersions, Environ. Sci. Technol. 41 (2007) 284–290.
[27] K.M. Buettner, C.I. Rinciog, S.E. Mylon, Aggregation kinetics of cerium oxide nanoparticles in monovalent and divalent electrolytes, Colloids Surf. A: Physicochem. Eng. Aspects 366 (2010) 74–79.
[28] H. Hyung, J.H. Kim, Natural organic matter (NOM) adsorption to multi-walled carbon nanotubes: effect of NOM characteristics and water quality parameters, Environ. Sci. Technol. 42 (2008) 4416–4421.
[29] B.V. Derjaguin, L. Landau, Theory of the stability of strongly charged lyophobic sols and of the adhesion of strongly charged particles in solution of electrolytes, Acta Physiochem. USSR 14 (1941) 633–662.
[30] E.J. Verwey, J.T. Overbeek, Theory of the Stability of Colloidal Dispersions, Elsevier, Amsterdam, 1948.
[31] D.A. Sverjensky, Zero-point-of-charge prediction from crystal chemistry and solvation theory, Geochim. Cosmochim. Acta 58 (1994) 3123–3129.
[32] N. Saleh, H.-J. Kim, T. Phenrat, K. Matyjaszewski, R.D. Tilton, G.V. Lowry, Ionic strength and composition affect the mobility of surface modified Fe0 nanoparticles in water saturated sand columns, Environ. Sci. Technol. 42 (2008) 3349–3355.
[33] N. Saleh, K. Sirk, T. Phenrat, B. Dufour, K. Matyjaszewski, R.D. Tilton, G.V. Lowry, Surface modifications enhance nanoiron transport and DNAPL targeting in saturated porous media, Environ. Eng. Sci. 27 (2007) 45–57.